HHS Public Access

Author manuscript

J Mol Biol. Author manuscript; available in PMC 2017 December 04.

Published in final edited form as:

J Mol Biol. 2016 December 04; 428(24 Pt B): 4890–4904. doi:10.1016/j.jmb.2016.10.033.

Structure of a PKA RIα Recurrent Acrodysostosis Mutant Explains Defective cAMP-dependent Activation

Jessica GH Bruystens[1], **Jian Wu**[1,2], **Audrey Fortezzo**[1], **Jason Del Rio**[2], **Cole Nielsen**[2], **Donald K. Blumenthal**[3], **Ruth Rock**[4], **Eduard Stefan**[4], and **Susan S. Taylor**[1,2,*]

[1]Department of Chemistry and Biochemistry, University of California at San Diego, La Jolla, CA 92093, USA

[2]Department of Pharmacology, University of California at San Diego, La Jolla, CA 92093, USA

[3]Department of Pharmacology and Toxicology, University of Utah, Salt Lake City, UT 84112, USA

[4]Institute of Biochemistry and Center for Molecular Biosciences, University of Innsbruck, Innrain 80/82, 6020 Innsbruck, Austria

Abstract

Most disease related mutations that impair PKA signaling are present within the regulatory PKA RI alpha-subunit (RIα). Although mutations in the PRKAR1A gene are linked to Carney complex disease (CNC) and more recently to acrodysostosis-1 (ACRDYS1), the two diseases show contrasting phenotypes. While CNC mutations cause increased PKA activity, ACRDYS1 mutations result in decreased PKA activity and cAMP resistant holoenzymes. Mapping the ACRDYS1 disease mutations reveals their localization to the second of two tandem cAMP binding domains (CNB-B) and here we characterize a recurrent deletion mutant where the last 14 residues are missing. The crystal structure of a monomeric form of this mutant (RIα92-365) bound to the C subunit reveals the dysfunctional regions of the RIα-subunit. Beyond the missing residues, the entire capping motif is disordered (residues 357-379) and explains the disrupted cAMP binding. Moreover, the effects of the mutation extend far beyond the CNB-B domain and include the active site and N-lobe of the C-subunit, which is in a partially open conformation with the C-tail disordered. A key residue that contributes to this crosstalk, D267, is altered in our structure and we confirmed its functional importance by mutagenesis. In particular, the D267 interaction with Arg241, a residue shown earlier to be important for allosteric regulation, is disrupted thereby strengthening the interaction of D267 with the C-subunit residue Arg194 at the R:C interface. We see here how the switch between active (cAMP-bound) and inactive (holoenzyme) conformations is perturbed and how the dynamically controlled crosstalk between the helical domains of the two CNB-domains is necessary for functional regulation of PKA activity.

*Correspondence: staylor@ucsd.edu (S.S.T.), Phone : 858 534-3677, Fax : 858-534-8193.

Accession Number

Coordinate and structure factors have been deposited in the Protein Data Bank with accession number of 5JR7.

Graphical abstract

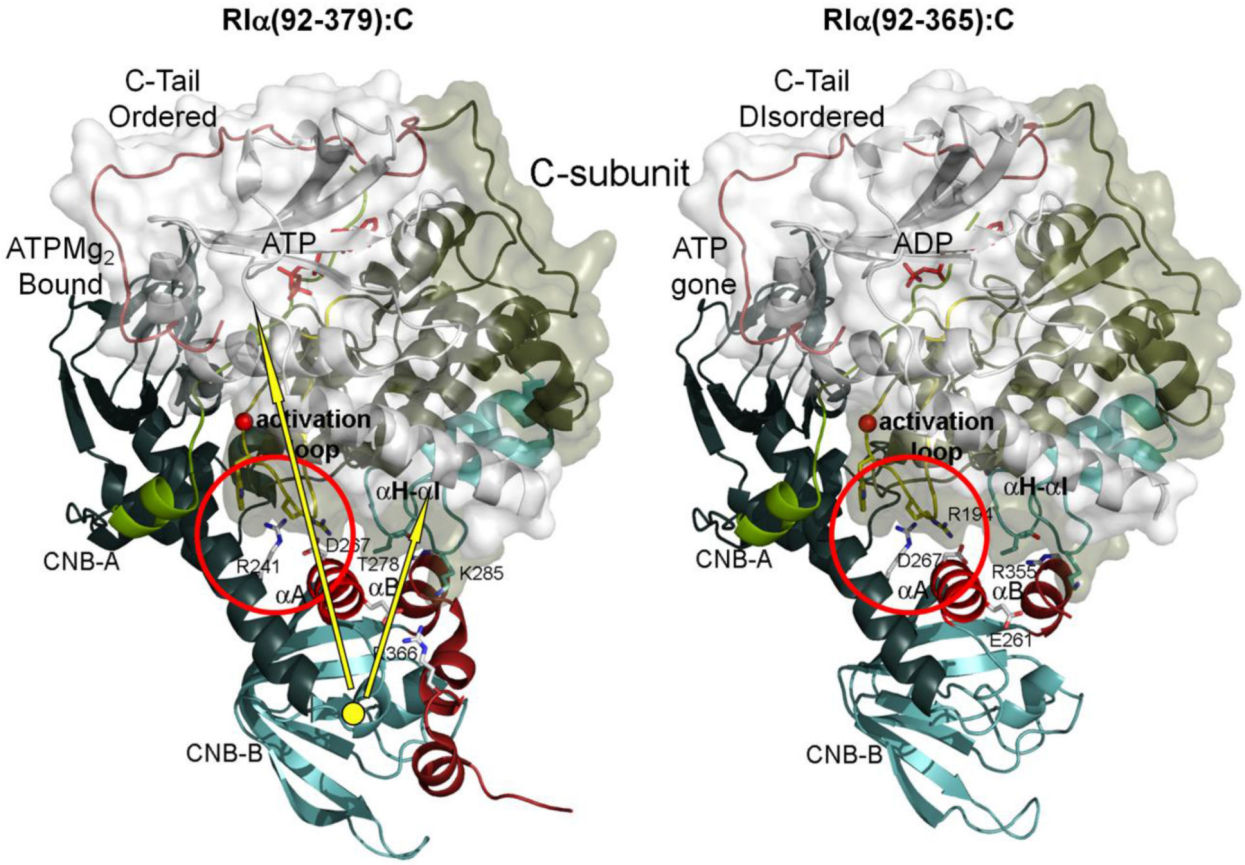

Keywords

PKA signaling; RIα subunit; disease mutations; crystal structure

Introduction

In the absence of cAMP protein kinase A (PKA) exists as an inactive complex composed of a regulatory (R) subunit dimer bound to two inhibited catalytic (C) subunits. Any mutation to the R-subunit that either enhances or abrogates PKA activity results in aberrant signaling and can cause memory defects, cancer, and endocrine disorders. The four PKA R-subunit isoforms (RIα, RIβ, RIIα, and RIIβ) share a general domain organization that includes the N-terminal dimerization/docking (D/D) domain, a linker containing the inhibitor site (IS), and two consecutive cAMP binding domains (CNB-A, CNB-B). The CNB domain has been conserved from bacteria to man and allows cells to convert the second messenger cAMP signal into a biological response. The phosphate binding cassette (PBC), embedded within a stable 8 stranded beta sandwich, contains a small helix and is the signature motif of all CNB domains. In addition there are two helical motifs that flank the beta sandwich. The N-terminal αN-αA motif precedes β1 while the αB-αC motif follows beta 8. In contrast to the stable beta motif, the three helical motifs undergo coordinated movements from the cAMP-

bound (active C subunit) to the holoenzyme (inhibited C subunit) conformations [1, 2]. However; the cAMP response profiles of the four R-subunit isoforms as well as knock-out phenotypes in mice are different. Only RIα(−/−) mice show embryonic lethality, indicating that RIα is pivotal and essential for survival [3, 4]. The fundamental importance of RIα is further supported by the observation that most diseases linked to PKA signaling are associated with RIα.

Carney Complex (CNC) disease is an autosomal-dominant syndrome associated with mutations in the PRKAR1A gene, which is the gene that codes for the RIα protein. A majority of the approximately 120 mutations discovered so far to cause the disease are subject to nonsense mediated mRNA decay (NMD), which leads to haplo-insufficiency of RIα protein levels and unregulated C subunit as the other R subunit isoforms fail to compensate [5]. But a few dysfunctional CNC mutants escape NMD and result in increased PKA activity as their holoenzymes show enhanced sensitivity to cAMP. In contrast to CNC, acrodysostosis (ACRDYS) patients display hormone resistance and lowered PKA activity with mutations found in the PRKAR1A gene (ACRDYS1) as well as the phosphodiesterase PDE4D gene (ACRDYS2) [6-8]. ACRDYS is a rare syndrome characterized by severe physical malformations due to skeletal dysplasia present already at birth. Short metacarpals and metatarsals of the hands and feet, cone-shaped epiphyses, midface hypoplasia, and overall short stature, are some physical disease characteristics [9, 10]. Developmental delay and intellectual disability also accompany some patients with this autosomal dominant syndrome [6, 7].

The RIα mutations associated with ACRDYS patients are a plausible molecular culprit for the disease [6, 7], and one particular mutation found in several unrelated patients is a deletion at the C-terminus of CNB-B that escapes NMD. Specifically, Arg366 becomes a stop codon which results in an expressed protein that is missing the last 14 residues [Δ366-379 RIα or RIα(1-365)]. To understand the molecular consequences of this deletion mutant as well as a less common ACRDYS1 deletion mutant [Δ371-379 RIα or RIα(1-370)] we used crystallography alongside biochemical and cellular analyses. We confirmed an increased requirement of cAMP for holoenzyme dissociation with biological assays, and small angle X-ray scattering (SAXS) showed conformational changes. Crystallization of a single representative structural unit, the ACRDYS heterodimer [RIα(92-365):C], showed that the entire capping motif at the C-terminus of the CNB-B domain is dysfunctional and changes go beyond just the deleted residues (residues 366-379), which can explain why this holoenzyme is defective in binding cAMP. In addition, however, the consequences of this mutation reach out to the inhibitor site at the active site cleft of the C-subunit and to the C-terminal tail of the C-subunit. In previous RIα heterodimers the pseudosubstrate inhibitor is locked into the active site cleft with ATP and 2 Mg ions, and the C-subunit is in a tightly closed conformation similar to PKI [1, 2, 11]. In contrast, the ACRDYS1 mutant has ADP bound weakly in the active site with no Mg^{++}, and the C-subunit is in a more open conformation with many features of the N-lobe, including the C-tail, being partially disordered. The mutant structure thus shows long range dynamic effects of the C-terminal cAMP binding motif.

Results

Mutational hot-spots of ACRDYS1

Mutations that have been found to be associated with ACRDYS are highlighted in Figures 1 and S1 and are clearly localized to the CNB-B domain. They are thought to be inhibitory and form holoenzymes that require more cAMP for activation. The location and frequency of the CNB-B point mutations highlight two of the most important features of the cAMP-binding domain, the PBC, which is the cAMP phosphate docking site, and the C-terminal hydrophobic capping motif for the adenine ring. The functional importance of these motifs is clear in the cAMP-bound conformation whereas both sites undergo a major structural rearrangement in the C subunit bound conformation [12]. In the holoenzyme both capping motifs are displaced by over 20Å from the PBC. We thus focused on two deletion mutants at the C-terminus that were detected in patients and have a dominant molecular outcome likely causing the disease phenotype of ACRDYS.

Activation of ACRDYS1 complexes requires more cAMP

To determine the effects of the ACRDYS1 mutations on cAMP activation we used two strategies. To investigate the functional consequences of the ACRDYS1 deletions *in vitro* we engineered and expressed both deletion mutants, RIα(1-365) and RIα(1-370) as well as a monomeric form of one of the mutants, RIα(92-365) in *E. coli*, and formed holoenzyme complexes with each. We then used a fluorescence polarization (FP) assay to measure activation of the purified complexes. To measure the consequences of the RIα(1-365) ACRDYS1 mutation and another ACDRYS1 mutation on PKA activation in intact cells we used a Protein-fragment Complementation Assay (PCA) [13-15].

The FP assay with full-length R_2C_2 holoenzymes confirmed *in vitro* that both deletion mutants are resistant to cAMP activation (Fig.2a). The heterodimer complex, RIα(92-365):C, is also resistant to activation by cAMP (Fig.2b). The larger deletion, RIα(1-365), showed a somewhat greater increase in EC_{50} for cAMP induced activation and the cooperativity of PKA activation by cAMP was reduced for RIα(1-365) (Fig.2a). Both deletions thus are defective in PKA activation, which is consistent with the ACDYS1 phenotype, and this feature is retained in the R:C heterodimer. Next, we applied the highly specific *Renilla* Luciferase (*R*luc) protein complementation assay (PCA) to analyze the consequences of the RIα mutations directly in living cells (Fig.S2a) [13-15]. We compared the protein:protein interactions (PPIs) of wild type RIα:PKAc complex formation directly with complexes involving two different ACRDYS1 mutants (RIα(1-365) and RIα-R333P). RIα-R333P, in contrast to the deletion mutant, is deficient in the docking site for the cAMP phosphate. We first quantified and compared basal cellular complex formation of these holoenzymes and showed higher PPI levels for the holoenzymes containing the two ACRDYS1 mutations (Fig.2c). To assess the impact of cellular cAMP elevation on the holoenzyme complexes, we used HEK293 cells that stably express the beta-2 adrenergic receptor (β_2AR), a prototypical GPCR which is coupled to cAMP production. This confirmed that both mutants were defective in activation by isopreternol.

SAXS analysis of acrodysostosis holoenzymes

To assess possible structural effects of the C-terminal ACRDYS1 mutations in solution, SAXS data was collected for full-length holoenzyme complexes formed with RIα(1-365) and RIα(1-370) and compared to previous SAXS data for wt RIα holoenzyme [16]. Based on the *I(q) versus q* and the linear Guinier plots, the samples were free of non-specific aggregation (Fig.2d and S3). The overall shape of the mutants is comparable to that of wild-type holoenzyme but the slightly longer (Gln370stop) ACRDYS1 protein suggests an increase in bilobal character. Both mutants and wt RIα have a major peak at ~40 Å and a shoulder around 110 Å; however, the RIα(1-370) mutant holoenzyme shows a much more pronounced shoulder that is shifted to ~100 Å.

Both mutants show a 10 Å reduction in D_{max} (130 Å), and their R_g values are also smaller (43.8 and 45.4 Å for Gln370stop and Arg365stop, respectively) compared to 47.1 Å for wt RIα. Due to the C-terminal truncations, a reduction in D_{max} might be expected, but the reductions in both R_g and D_{max} were surprisingly large and indicative of significant compaction of the mutant holoenzymes in solution compared to wt RIα.

Overall structure of the acrodysostosis R:C heterodimer

To investigate structural consequences of the Acrodysostosis deletion in more detail we expressed the monomeric form, RIα(92-365), and formed a heterodimer complex RIα(92-365):C. After characterizing the heterodimer biochemically, the structure was solved to 3.5 Å resolution (Supplement Table S1). The crystals contain two molecules per asymmetric unit and show different packing compared to our previous R:C heterodimer (Fig. S4).

Because the ACRDYS1 construct is missing 14 residues at the C-terminus (residues 366-379) Arg366, which is part of a holoenzyme-specific salt-bridge, and Tyr371, the capping residue for CNB-B, are missing (Fig. 3). However, additional residues beyond the deletion are now also disordered. The electron density for one chain (chain B) ends at Gly358 and the other (chain D) at Leu357. Thus in both molecules the entire αC helical region is disordered even though residues 358-365 are present in the construct (Fig. 3b and Fig. 4).

As seen in previous structures, extension of the αB/C-helix in CNB-A in the holoenzyme creates a large buried surface area between the subunits (Fig. 3b and Fig. 5a). In addition to the inhibitor site (IS) at the active site cleft of the C-subunit, two other regions in the C-subunit contribute to this interface - the activation loop (AL) and the αH-αI loop. The AL (Fig. 5a) interacts with residues from the extended αB/C-helix in CNB-A and the αA-helix of CNB-B while the αB helix in CNB-B interacts directly with the αH-αI loop in the C-lobe of the C-subunit (Fig. 5c). Subtle changes in both interfaces emphasize the extended allosteric network of this complex and are outlined in the following section.

Furthermore, the effects of the mutation extend beyond the C-terminus. They reach to the active site cleft of the C-subunit where ATP is no longer bound even though it is present in the crystallization buffer. Instead we find no Mg^{++} ions and ADP bound loosely at the active site cleft with the C-subunit in a partially open or intermediate conformation. The C-Tail of

the C-subunit is partially disordered, key links between the glycine-rich loop (G-Loop) and the C-tail are disordered, and the conserved electrostatic link between the Lys72 and Glu91 is broken. These long range consequences are described in more detail below.

Changes in the network nucleated by the C-Terminal capping motif

In the cAMP-bound conformation every PKA R-subunit forms an extended αC-helix at the C-terminus that localizes the capping residue, Y371, onto the adenine ring of cAMP (Fig. 1c). In the holoenzyme this segment rearranges to form an αC'/C" kinked helix. This entire αC'/C"-helix, including Y371, is missing in the mutant (Fig. 4). The ACRDYS mutant protein has a stop codon in place of Arg366, which forms a holoenzyme-specific salt bridge to E261 in the αA-helix of CNB-B in the wild type protein. This αA-helix also contains the capping residue for CNB-A, W260. Thus the deletion removes the capping residue for CNB-B as well as the direct link to the capping residue for CNB-A (Fig. S2b). The αA-helix in the CNB-B domain contains another important conserved residue at its C-terminus, D267. Asp267 in the wild-type like RIα(91-379) complex is hydrogen bonded to Arg241 in the extended αB/C-helix of CNB-A. Arg241, also conserved in every R-subunit, was shown previously to contribute to cAMP binding and allostery in RIα [17]. In our mutant the side chain of D267 no longer interacts with R241 (Fig. 6c and Fig. 7).

αB-helix in CNB-B interacts with the αH-αI loop in the C-subunit—Although the salt bridge is missing, the RIα-subunit is still in an extended holoenzyme conformation, and the R:C interface is conserved (Fig. 5). In part this is due to two αB-helix residues, Arg355 and Arg352, that H-bond to two residues in the αH-αI loop, Asp276 and Thr278 (Fig. 5c). Both arginines are conserved in RIα and RIβ, whereas RII-subunits have only Arg355; Arg352 is replaced with Ala. This is the most C-terminal region of RIα that contributes to the R:C interface (Fig. 5c), and without the cap-induced switch it apparently cannot be easily released by cAMP even though the salt bridge is broken. The side chain of Lys285 in the C-subunit, which typically H-bonds to Arg355 in RI holoenzymes, is also part of this interface; it is solvent-exposed and dynamic in our structure (Fig. 5c).

αA-helix in CNB-B interacts with the Activation Loop in the C-subunit—The αA-helix of CNB-B also forms a major interface with the Activation Loop of the C-subunit in the holoenzyme (Fig. 5a). Multiple tryptophans and arginines contribute to this interface, and communicating to this network of interactions mediates the release of the C-subunit when cAMP binds to the first CNB-B domain. Figure 5a also shows how the N3A motif of CNB-B is fused directly to the B/C-helix of CNB-A. It is the switch between the helical motifs in each CNB domain that likely contributes to the allosteric activation of the holoenzyme, and this communication is clearly disrupted in this mutant according to the FP data (Fig. 2).

Functional importance of D267

While the importance of Arg241 for allostery was previously described [17], the importance of D267 has not been addressed. To confirm the importance of this residue we mutated D267 to Ala and assayed its properties in cells using the *R*lucPCA reporter to quantify PPI dynamics of the type I PKA holoenzyme. The results show that the D267A mutation does

form a complex with PKA-C in cells. However, the holoenzyme is more resistant to activation by isoproterenol, confirming that D267 is essential for mediating communication between the CNB-B and CNB-A domains (Fig. 6a). Similar to the ACRDYS1 mutants, the activation by cAMP is significantly impaired in the holoenzyme form with RIα-D267A. The dose response to isoproterenol is similar to the ACRDYS1 deletion mutant (Fig. 6b). These data confirm that both ACRDYS1-relevant PKA holoenzyme complexes [RIα-D267A:PKAc and RIα(1-365):PKAc] are less responsive to GPCR-triggered cAMP activation.

Dynamic changes in the C-subunit

Surprisingly, our R:C complex also captured an intermediate conformational state of the C-subunit. Previous structures of RIα:C complexes showed the linker and inhibitor site locked by ATP into the active site cleft (Fig. S5a). In our structure the active site is more open, there is no density for the gamma phosphate of ATP or metal ions, and the N-lobe is in a more open conformation.

Nucleotide—The inhibitor site within the linker, which is flexible and disordered in the RIα dimer [18], typically becomes ordered in the holoenzyme by anchoring to the active site cleft of the C-subunit. In wt RIα, ATP binds with high affinity to this site because RIα is a pseudosubstrate inhibitor like PKI [1, 19]. In our structure the inhibitor site shows several differences. Most noteworthy is the electron density pointing towards the presence of ADP instead of ATP, even though ATP was included in the crystallization buffer; (Fig. S5b). Of the two R:C heterodimers within the ASU, the 2Fo-Fc map at 1σ for chain A shows reasonable density for ADP whereas chain C has poor density even for ADP. Neither chain has density for any magnesium ions.

Inhibitor site—The RIα linker is also more dynamic than in previous structures (Fig. S5c and 8a,b). There is weak density for the side chains of the inhibitor sequence (Arg94-Arg-Gly-Ala-Ile98). While Arg94 is usually part of a hydrogen bond cluster with three C-subunit residues (Tyr330, Glu127, and Thr51), it is disordered in our structure, providing further evidence for an overall more solvent-accessible active site.

N-Lobe—Although alignment of the two C-subunits from the ASU (chain A and chain C) show that they are very similar, a closer look reveals some differences. Comparison with an ATP/Mg^{+2}-bound ternary complex, an ADP-bound intermediate, and a completely open apo C-subunit structure highlights these differences (Fig. 8c,d). Movements of the G-loop in various C-subunit states are a good indicator of closed, open and intermediate conformational states. When bound to ADP and one Mg ion, the G-loop is in an intermediate conformation [20], and this is similar to our structure (Fig. 8c).There is also little density for Phe54, a G-loop residue that is usually well-resolved in most structures.

C-Tail—The C-Tail also shows differences. Phe327 and Tyr330 interact with the adenine and ribose rings of ATP, respectively, and are an essential part of the ATP binding pocket [21]. In our structure, chain A shows density for both aromatic residues while the density for these residues in chain B is poor (Fig. 8d and S5d). Density for the C-terminal hydrophobic motif (Phe347 and Phe350) is also weak in chain B. The recently published ADP-bound C-

subunit shows increased flexibility of the C-tail, and this is similar to our structure [20]. Thus the C-tail is largely disordered. The flexibility of the C-tail also disrupts the link between Arg56 in the G-loop and Glu333 in the C-tail. Finally the conserved Lys in β strand 3 (K72), which forms a highly conserved salt bridge to Glu91 in the αC-helix in all protein kinases, is disordered. Multiple lines of evidence thus indicate that the N-Lobe is much more dynamic and in an intermediate conformation.

Discussion

The fact that most disease mutations associated with PKA signaling are localized in the RIα subunit emphasizes the unique importance of RIα for regulating PKA function in cells. RIα mutations that escape NMD are indicated in Figure 9b, and the clustering of these mutations highlights the distinct functional roles of the two CNB domains. The activating CNC mutations are clustered mostly in CNB-A, which has extended direct interactions with the C-subunit. Other previously analyzed, non-disease related mutations that lie directly at the R:C interface also create complexes that are easier to activate *in vitro* (R226A, L233A, M234A) (Fig. S6) [22]. In contrast, inhibitory ACRDYS1 mutations are clustered in CNB-B. The Arg333Lys mutation in CNB-B was originally discovered in S49 mouse lymphoma cells and reduces cAMP affinity by reducing the on-rate for cAMP [23-27]. Previous kinetic studies as well as mutations of the essential PBC Arg in CNB-A (Arg209) and CNB-B (Arg333) led to a model for cooperative activation of the RIα holoenzyme where cAMP binds first to CNB-B [27-29]. This mechanism is consistent with the R:C heterodimer structure [1, 2], is supported by urea denaturation studies [30], and was quantitatively confirmed recently by MD simulations [31]. Although the molecular mechanisms are likely different, all ACRDYS1 mutations lead to a desensitized enzyme that is resistant to activation by cAMP, providing further evidence for the “gatekeeper” role of the CNB-B domain.

ACRDYS1 mutations specifically highlight the importance of the PBC and the hydrophobic capping motif. In the cAMP-bound conformation (Fig. 1c) a conserved Arg in the PBC anchors the phosphate of cAMP, a conserved Glu in the PBC anchors the ribose-OH, and a hydrophobic residue caps the adenine ring of cAMP. Two of these residues in CNB-B harbor ACRDYS1 mutations (Arg333Leu/Pro/Cys and Tyr371His/Cys). Several other single site ACRDYS1 mutations cluster around the PBC (Gln283Arg and Gly287Glu) or are part of it (Ile325Thr, Ala326Val and Arg333Leu/Pro/Cys) (Fig. 9b and S1) [32-34]. In addition to the ACRDYS1 mutations from patients, we showed with mutagenesis in previous mechanistic studies their effect on PKA activation (Fig.S6). Mutating Tyr371, one of the capping residues for example, reduces the affinity for cAMP most likely by increasing the off rate [1]. Mutating either of the PBC arginines or the two capping residues also makes the R-subunit harder to activate and the importance of these residues is now also confirmed with the disease mutations [23, 24, 28, 29].

Furthermore, the ACRDYS1 mutations point to the importance of the coordinated motions of the helical motifs that are embedded within each CNB domain. While the β-barrel that harbors the PBC does not undergo conformational changes, the helical subdomain does. These motions in each CNB domain associated with the binding and release of cAMP were

described previously [1, 2] and revealed how they specifically create the R:C interface in the holoenzyme. Upon cAMP binding to CNB-B, which is the initial step in activation, the αB-helix moves “in” allowing Y371 in the now extended αC-helix to cap the adenine ring of cAMP while the αA-helix moves “out” with a broken E261-R366 salt bridge to deliver the capping residue (Trp260) to cAMP in CNB-A (Fig. 9c). In the holoenzyme conformation the αB-helix of CNB-B is docked onto the αH-αI loop of the C-subunit while the extended αB/C-helix of CNB-A and the αA-helix of CNB-B provide the docking surface for the Activation Loop of the C-subunit (Fig. 9a). Three residues of the αA-helix (Trp260, Leu263, and Asp267) contribute to this docking surface. While electrostatic interactions between D267 and R241 are rearranged but maintained in both structures, the partner for the hydrophobic node created by Leu263 and Trp260 is different. Instead of docking onto the activation loop of the C-subunit this hydrophobic node switches to cap cAMP bound to CNB-A.

There is thus a line of communication from the PBC in CNB-B to the Activation Loop and the active site cleft as well as indirectly to the N-Lobe and the C-Tail of the C-subunit. The αA-helix of CNB-B is a centerpiece for this allosteric network, and our mutation of the conserved D267 at the end of the αA-helix confirmed the importance of this allosteric node. In contrast to single site mutations, some now observed in patients, we focus here on a C-terminal deletion mutant that not only alters the cAMP binding site but also severs the cross talk between the cAMP binding site and the αA and αB helices. Our mutant has a different mechanism compared to simply changing the PBC arginines. Thus, our structure highlights the network of crosstalk that links docking of cAMP to the C-terminus of CNB-B to the regulation of the αB/C-helix dynamics through the positioning of a key aspartic acid in the αA-helix of CNB-B. The removal of the αC-helical motif appears to uncouple the signal to unlock the CNB-A domain thus preventing it from transitioning into its cAMP bound conformation. In our ACRDYS1 structure the side chain of D267 is rotated to favor its interaction with Arg194 in the Activation Loop of the C-subunit and away from Arg241, which is a key allosteric residue that mediates the kinking of the B/C-helix. (Fig. 7).

The consequences of the ACRDYS1 deletion extend across the entire molecule. Even though the E261 to R366 salt bridge is broken, the interface with the αH-αI loop is intact (Fig. 5c). The extended interface with the activation loop is also in place, but D267 no longer favors interactions with Arg241; instead it faces Arg194 in the activation loop of the C-subunit (Fig. 5a). Arg241 is the only residue in the wild type enzyme that is part of a salt bridge between the two CNB domains, and this residue was predicted from earlier kinetic studies to be a key allosteric link between CNB-A and CNB-B [17]. Breaking the αB/C-helix in CNB-A is an essential requirement for conversion to the cAMP bound conformation, and it appears that D267 must toggle between Arg194 in the C-subunit and Arg241 in the αB/C-helix for this change to happen. In the absence of the C-terminal capping motif this switch mechanism is broken. As a consequence, ATP is also no longer bound tightly to the active site, the inhibitor peptide is loosely anchored, the glycine-rich loop is in a more open conformation and the C-Tail is more disordered (Fig. 8).

While further studies will be required to map the details of the allosteric network that links the CNB-B domain to holoenzyme activation, the deletion highlights the importance of the

αA-helix of CNB-B which contains the three essential and conserved residues: Trp260, the capping residue for CNB-A, Glu261, part of the salt bridge that links the αA-helix directly to Arg366 in the C-terminal capping motif, and Asp267, which interacts with the critical allosteric arginine, Arg241. Since Arg366 is missing in this mutant, there is no longer any direct communication between the αA-helix and the αC-helix. Another consequence of this mutation is that the critical link between Arg241 and Asp267 is broken. Without the C-terminal helical motif, the signal to disengage from the C subunit is apparently not transmitted. Instead the equilibrium favors the holoenzyme conformation even though ATP is no longer tightly bound at the active site. We have captured here a dynamic state of the R:C interface, and this contributes to the uncoupling of ATP at the active site cleft and the subsequent opening of the N-Lobe. Using the protein complementation assay we confirmed the importance of D267 as part of an allosteric hot-spot that links cAMP binding to the CNB-B domain to PKA activation. In addition, after the submission of this manuscript D267G was actually identified as an ACRDYS1 mutation in a patient, further confirming the importance of this residue [35].

The disease mutations associated with CNC and ACRDYS1 highlight the complex and extended network of communication that exists between the two domains and provide mechanistic insight into how these domains switch between their cAMP bound state where the kinase is active and the holoenzyme state where the catalytic activity is inhibited. Hopefully structures of additional disease mutations as well as MD simulations will further resolve the conformational dynamics that lead to allosteric activation of RIα. Our structure of the ACRDYS1 mutant is thus a significant first step that emphasizes not only the importance but also the complexity of coordinated long-range dynamics.

Materials and Methods

Protein Expression and Purification

Bovine full-length wild-type (1-379), deletion mutant Δ366-379, deletion mutant Δ371-379, and double deletion mutant Δ1-91 + Δ366-379 RIα proteins were purified as described previously [36, 37]. The acrodysostosis mutation constructs Δ366-379, Δ371-379, and Δ1-91 + Δ366-379 were generated by QuickChange site-directed mutagenesis. Murine catalytic subunit of PKA was purified as documented previously [38].

Holoenzyme Formation

Mutant and wild-type holoenzymes were formed by combining R and C subunits in a 1.2 to 1 molar ratio followed by two 24 hour dialysis in holoenzyme buffer (10 mM Mops pH 7, 50 mM NaCl, 2mM $MgCl_2$, 0.2 mM ATP, 1 mM TCEP-HCl). To isolate the complex the dialyzed protein was run over an S200 gel filtration column and resulted in a > 96% pure R:C preparation.

PKA Activation / IP-20

The holoenzymesactivation was investigated by a fluorescence polarization assay [39]. Holoenzymes were formed with molar ratio of 1.2 mol RIα to 1 mol C subunit and diluted in buffer containing 20 mM Hepes (pH 7), 75 mM KCl, 0.005% Triton X-100, 1 mM ATP, 1

mM DTT, and 10 mM $MgCl_2$. A 20-residue long PKA inhibitor peptide (IP-20) labeled with succinimidyl activated carboxyfluorescein (FAM-IP20) was added to RIα holoenzymes, followed by addition of cAMP to activate PKA. The working concentration of C subunit was 12nM, FAM-IP20 was 2nM, and 2-fold serial dilutions from 2000 - 0 nM cAMP were added to initiate holoenzyme dissociation and FAM-IP20 binding to the C subunit. Fluorescence polarization readings with excitation at 485 nm and emission at 535 nm were carried out with a GENios Pro micro-plate reader (Tecan) using black flat-bottom Costar® assay plates. Each protein was tested in quadruplicate and the data were analyzed with Prism 4.

Crystallization and Structure Determination of the Acrodysostosis Δ1-91 +Δ366-379 RIα:C Heterodimer

Purified RIα(92-365) was combined with purified C-subunit peak 1 to make the heterodimer complex as described above. The purified complex was concentrated to 10 mg/ml and then centrifuged at 14,000 rpm for 10 minutes. Crystallization trays were set up by hanging-drop vapor diffusion with various commercially available screens at 50% protein plus 50% screen buffer at 22°C. Several crystal hits were obtained with the best condition that yielded a 3.56Å structure being composed of 0.2 M Sodium thiocyanate and 20% PEG3350 with the protein at a final concentration of 5 mg/ml in a 1.6 μl drop.

Crystals were flash frozen after soaking in a cryoprotectant composed of mother liquor supplemented with 15% Glycerol. X-ray diffraction data sets were collected at the Advanced Light Source, Berkeley California beamline 8.2.2 from one crystal and processed with HKL2000 [40]. This resulted in a P_1 space group and cell dimensions of a=60.1 Å, b=66.8 Å, and c=87.9 Å (Table S1). The best dataset resulted in a structure solution with final resolution of 3.56 Å. The structure was solved using the RIα:C heterodimer structure (pdb 2qcs) as a molecular replacement probe and the last 14 residues deleted [1].

While crystallization was carried out in the presence of ATP/Mg, the F_o-F_c density at 3σ level indicates ADP to be in the active site of two C-subunit molecules in the ASU. In addition, electron density for Mg ions cannot be located. The final model includes residues 92-357 for the R-subunit, residues 13 to 350 of the C-subunit and ADP with 80% occupancy. The R and R-free are 0.251 and 0.308 respectively, and the structure model has a good geometry as evaluated with PROCHECK [41] (Table S1).

Small Angle X-ray Scattering

Holoenzymes were purified as described above and the final buffer composition was 10 mM Mops pH 7, 50 mM NaCl, 2 mM $MgCl_2$, 1 mM TCEP-HCl and 0.2 mM ATP. Immediately prior to the SAXS experiments purified holoenzyme complexes were concentrated to a final concentration of ~8-12 mg/ml using using 30,000 MWCO Millipore concentrators then filtered using 0.2 micron Z-spin microfuge filters. The SAXS data were collected for 90 min for the wild-type and mutant samples. SAXS data were acquired at 12 °C using the SAXSess (Anton Paar) line collimation (10 mm) instrument at the University of Utah. Data were collected using an image plate detector and normalized buffer subtraction and data reduction to I(q) versus q ($q = (4\pi\sin\theta)/\lambda$; 2θ is the scattering angle; λ = 1.54 Å CuK_α) was carried out using the program SAXSquant 2.0. P(r) functions for the experimental and

theoretical scattering were calculated using GNOM (as implemented in ATSAS 2.5.0; [42]). The experimental scattering data were corrected for smearing effects in GNOM using beam length profile parameters measured at the time of protein data collection. The theoretical scattering profile for the Δ366-379 RIα$_2$:C$_2$ complex crystal structure was calculated using CRYSOL.

Renilla luciferase PCA measurements of cellular PPIs

HEK293 cells stably expressing the β_2AR were grown in DMEM supplemented with 10% FBS [13-15]. We transiently overexpressed combinations of indicated *R*luc PCA based reporter constructs in 24 well plates. Following treatments of attached HEK293 cells with increasing concentrations of isoproterenol for 15 minutes we exchanged the growth medium and resuspended HEK293 cells in PBS 48 hours post-transfection for the *R*luc PCA measurements. Cell suspensions were transferred to 96-well plates and subjected to bioluminescence analysis using the LMaxTM^{II}384 luminometer (Molecular Devices). *R*luc bioluminescence signals were integrated for 10 seconds following addition of the *R*luc substrate benzyl-coelenterazine (5 μM; Nanolight). We performed the *R*luc PCA PPI analyses using human RIα (NP_002725.1) and mouse PKAc (C). We have analyzed following mutations which are indicated with the bovine RIα numbering (R239A=human R241, D267A=human D269; R333P=human R335, RIα(1-365)=human RIα(1-367)). We generated the indicated *R*luc PCA fused mutants of RIα using site directed mutagenesis.

Supplementary Material

Refer to Web version on PubMed Central for supplementary material.

Acknowledgements

This work was funded in part by NIH grant GM 034921 to S. S. Taylor. The Advanced Light Source is supported by the Director, Office of Science, Office of Basic Energy Sciences, of the U.S. Department of Energy under Contract No. DE-AC02-05CH11231. We thank Dr. Mira Sastri for comments of our manuscript, Alexandr Kornev for help of our manuscript preparation, and Dr. Jill Trewhella for the generous use of small-angle scattering and laboratory facilities at the University of Utah. X-ray scattering data were collected at the University of Utah using facilities that were supported by United States Department of Energy Grant DE-FG02-05ER64026 (to Jill Trewhella). E.S. was supported by grants from the Austrian Science Fund (FWF, P27606; SFB-F44).

Abbreviations

PKA	cAMP protein kinase A
CNC	Carney complex disease
ACRDYS1	acrodysostosis-1
CNB	cAMP binding domains

References

[1]. Kim C, Cheng CY, Saldanha SA, Taylor SS. PKA-I holoenzyme structure reveals a mechanism for cAMP-dependent activation. Cell. 2007; 130:1032–1043. [PubMed: 17889648]

[2]. Kim C, Xuong NH, Taylor SS. Crystal structure of a complex between the catalytic and regulatory (RIalpha) subunits of PKA. Science. 2005; 307:690–696. [PubMed: 15692043]

[3]. Boshart M, Weih F, Nichols M, Schutz G. The tissue-specific extinguisher locus TSE1 encodes a regulatory subunit of cAMP-dependent protein kinase. Cell. 1991; 66:849–859. [PubMed: 1832337]

[4]. Jones KW, Shapero MH, Chevrette M, Fournier RE. Subtractive hybridization cloning of a tissue-specific extinguisher: TSE1 encodes a regulatory subunit of protein kinase A. Cell. 1991; 66:861–872. [PubMed: 1889088]

[5]. Greene EL, Horvath AD, Nesterova M, Giatzakis C, Bossis I, Stratakis CA. In vitro functional studies of naturally occurring pathogenic PRKAR1A mutations that are not subject to nonsense mRNA decay. Hum Mutat. 2008; 29:633–639. [PubMed: 18241045]

[6]. Nagasaki K, Iida T, Sato H, Ogawa Y, Kikuchi T, Saitoh A, et al. PRKAR1A mutation affecting cAMP-mediated G protein-coupled receptor signaling in a patient with acrodysostosis and hormone resistance. J Clin Endocrinol Metab. 2012; 97:E1808–1813. [PubMed: 22723333]

[7]. Linglart A, Menguy C, Couvineau A, Auzan C, Gunes Y, Cancel M, et al. Recurrent PRKAR1A mutation in acrodysostosis with hormone resistance. N Engl J Med. 2011; 364:2218–2226. [PubMed: 21651393]

[8]. Michot C, Goff C, Goldenberg A, Abhyankar A, Klein C, Kinning E, et al. Exome sequencing identifies PDE4D mutations as another cause of acrodysostosis. Am J Hum Genet. 2012; 90:740–745. [PubMed: 22464250]

[9]. Ablow RC, Hsia YE, Brandt IK. Acrodysostosis coinciding with pseudohypoparathyroidism and pseudo-pseudohypoparathyroidism. AJR Am J Roentgenol. 1977; 128:95–99. [PubMed: 188348]

[10]. Le Stunff C, Tilotta F, Sadoine J, Le Denmat D, Briet C, Motte E, et al. Knock-in of the Recurrent R368X Mutation of PRKAR1A that Represses cAMP-Dependent Protein Kinase A Activation: A Model of Type 1 Acrodysostosis. J Bone Miner Res. 2016

[11]. Zheng J, Knighton DR, Xuong NH, Taylor SS, Sowadski JM, Ten Eyck LF. Crystal structures of the myristylated catalytic subunit of cAMP-dependent protein kinase reveal open and closed conformations. Protein Sci. 1993; 2:1559–1573. [PubMed: 8251932]

[12]. Berman HM, Ten Eyck LF, Goodsell DS, Haste NM, Kornev A, Taylor SS. The cAMP binding domain: An ancient signaling module. P Natl Acad Sci USA. 2005; 102:45–50.

[13]. Rock R, Bachmann V, Bhang HE, Malleshaiah M, Raffeiner P, Mayrhofer JE, et al. In-vivo detection of binary PKA network interactions upon activation of endogenous GPCRs. Scientific reports. 2015; 5:11133. [PubMed: 26099953]

[14]. Rock R, Mayrhofer JE, Bachmann V, Stefan E. Impact of kinase activating and inactivating patient mutations on binary PKA interactions. Frontiers in pharmacology. 2015; 6:170. [PubMed: 26347651]

[15]. Stefan E, Aquin S, Berger N, Landry CR, Nyfeler B, Bouvier M, et al. Quantification of dynamic protein complexes using Renilla luciferase fragment complementation applied to protein kinase A activities in vivo. Proceedings of the National Academy of Sciences of the United States of America. 2007; 104:16916–16921. [PubMed: 17942691]

[16]. Heller WT, Vigil D, Brown S, Blumenthal DK, Taylor SS, Trewhella J. C subunits binding to the protein kinase A RI alpha dimer induce a large conformational change. J Biol Chem. 2004; 279:19084–19090. [PubMed: 14985329]

[17]. Symcox MM, Cauthron RD, Ogreid D, Steinberg RA. Arg-242 is necessary for allosteric coupling of cyclic AMP-binding sites A and B of RI subunit of cyclic AMP-dependent protein kinase. J Biol Chem. 1994; 269:23025–23031. [PubMed: 8083203]

[18]. Bruystens JG, Wu J, Fortezzo A, Kornev AP, Blumenthal DK, Taylor SS. PKA RIalpha homodimer structure reveals an intermolecular interface with implications for cooperative cAMP binding and Carney complex disease. Structure. 2014; 22:59–69. [PubMed: 24316401]

[19]. Herberg FW, Taylor SS. Physiological inhibitors of the catalytic subunit of cAMP-dependent protein kinase: effect of MgATP on protein-protein interactions. Biochemistry. 1993; 32:14015–14022. [PubMed: 8268180]

[20]. Bastidas AC, Wu J, Taylor SS. Molecular features of product release for the PKA catalytic cycle. Biochemistry. 2015; 54:2–10. [PubMed: 25077557]

[21]. Yang J, Kennedy EJ, Wu J, Deal MS, Pennypacker J, Ghosh G, et al. Contribution of non-catalytic core residues to activity and regulation in protein kinase A. J Biol Chem. 2009; 284:6241–6248. [PubMed: 19122195]

[22]. Sjoberg TJ, Kornev AP, Taylor SS. Dissecting the cAMP-inducible allosteric switch in protein kinase A RIalpha. Protein Sci. 2010; 19:1213–1221. [PubMed: 20512974]

[23]. Steinberg RA, Russell JL, Murphy CS, Yphantis DA. Activation of type I cyclic AMP-dependent protein kinases with defective cyclic AMP-binding sites. J Biol Chem. 1987; 262:2664–2671. [PubMed: 3029091]

[24]. Murphy CS, Steinberg RA. Hotspots for spontaneous and mutagen-induced lesions in regulatory subunit of cyclic AMP-dependent protein kinase in S49 mouse lymphoma cells. Somat Cell Mol Genet. 1985; 11:605–615. [PubMed: 3000002]

[25]. Huang LJ, Taylor SS. Dissecting cAMP binding domain A in the RIalpha subunit of cAMP-dependent protein kinase. Distinct subsites for recognition of cAMP and the catalytic subunit. J Biol Chem. 1998; 273:26739–26746. [PubMed: 9756917]

[26]. Canaves JM, Leon DA, Taylor SS. Consequences of cAMP-binding site mutations on the structural stability of the type I regulatory subunit of cAMP-dependent protein kinase. Biochemistry. 2000; 39:15022–15031. [PubMed: 11106480]

[27]. Herberg FW, Taylor SS, Dostmann WR. Active site mutations define the pathway for the cooperative activation of cAMP-dependent protein kinase. Biochemistry. 1996; 35:2934–2942. [PubMed: 8608131]

[28]. Ogreid D, Doskeland SO. The kinetics of association of cyclic AMP to the two types of binding sites associated with protein kinase II from bovine myocardium. FEBS Lett. 1981; 129:287–292. [PubMed: 6269882]

[29]. Øgreid D, Døskeland SO. The Kinetics of the Interaction Between Cyclic AMP and the Regulatory Moiety of Protein Kinase II. FEBS Lett. 1981; 129:282–286. [PubMed: 6269881]

[30]. Leon DA, Canaves JM, Taylor SS. Probing the multidomain structure of the type I regulatory subunit of cAMP-dependent protein kinase using mutational analysis: role and environment of endogenous tryptophans. Biochemistry. 2000; 39:5662–5671. [PubMed: 10801316]

[31]. Boras BW, Kornev A, Taylor SS, McCulloch AD. Using Markov state models to develop a mechanistic understanding of protein kinase A regulatory subunit RIalpha activation in response to cAMP binding. J Biol Chem. 2014; 289:30040–30051. [PubMed: 25202018]

[32]. Linglart A, Fryssira H, Hiort O, Holterhus PM, Perez de Nanclares G, Argente J, et al. PRKAR1A and PDE4D mutations cause acrodysostosis but two distinct syndromes with or without GPCR-signaling hormone resistance. J Clin Endocrinol Metab. 2012; 97:E2328–2338. [PubMed: 23043190]

[33]. Lee H, Graham JM Jr. Rimoin DL, Lachman RS, Krejci P, Tompson SW, et al. Exome sequencing identifies PDE4D mutations in acrodysostosis. Am J Hum Genet. 2012; 90:746–751. [PubMed: 22464252]

[34]. Muhn F, Klopocki E, Graul-Neumann L, Uhrig S, Colley A, Castori M, et al. Novel mutations of the PRKAR1A gene in patients with acrodysostosis. Clin Genet. 2013; 84:531–538. [PubMed: 23425300]

[35]. Elli FM, Bordogna P, de Sanctis L, Giachero F, Verrua E, Segni M, et al. Screening of PRKAR1A and PDE4D in a Large Italian Series of Patients Clinically Diagnosed With Albright Hereditary Osteodystrophy and/or Pseudohypoparathyroidism. J Bone Miner Res. 2016; 31:1215–1224. [PubMed: 26763073]

[36]. Su Y, Dostmann WR, Herberg FW, Durick K, Xuong NH, Ten Eyck L, et al. Regulatory subunit of protein kinase A: structure of deletion mutant with cAMP binding domains. Science. 1995; 269:807–813. [PubMed: 7638597]

[37]. Wu J, Jones JM, Nguyen-Huu X, Ten Eyck LF, Taylor SS. Crystal structures of RIalpha subunit of cyclic adenosine 5′-monophosphate (cAMP)-dependent protein kinase complexed with (Rp)-adenosine 3′,5′-cyclic monophosphothioate and (Sp)-adenosine 3′,5′-cyclic monophosphothioate, the phosphothioate analogues of cAMP. Biochemistry. 2004; 43:6620–6629. [PubMed: 15157095]

[38]. Gangal M, Cox S, Lew J, Clifford T, Garrod SM, Aschbaher M, et al. Backbone flexibility of five sites on the catalytic subunit of cAMP-dependent protein kinase in the open and closed conformations. Biochemistry. 1998; 37:13728–13735. [PubMed: 9753461]

[39]. Saldanha SA, Kaler G, Cottam HB, Abagyan R, Taylor SS. Assay principle for modulators of protein-protein interactions and its application to non-ATP-competitive ligands targeting protein kinase A. Anal Chem. 2006; 78:8265–8272. [PubMed: 17165815]

[40]. Otwinowski Z, Minor W. Processing of X-ray diffraction data collection in oscillation mode. Macromolecular Crystallography. 1997; 276:307–326.

[41]. M. MW, Laskowski RA, Moss DS, Thornton JM. PROCHECK - a program to check the stereochemical quality of protein structures. J App Cryst. 1993; 26:283–291.

[42]. Svergun DI. Determination of the regularization parameter in indirect-transform methods using perceptual criteria. J Appl Crystallogr. 1992; 25:495–503.

[43]. Vigil D, Blumenthal DK, Heller WT, Brown S, Canaves JM, Taylor SS, et al. Conformational differences among solution structures of the type Ialpha, IIalpha and IIbeta protein kinase A regulatory subunit homodimers: role of the linker regions. J Mol Biol. 2004; 337:1183–1194. [PubMed: 15046986]

Highlights

- PKA, ubiquitous in mammalian cells, controls many biological processes, and RIa is a major target for diseases associated with PKA signaling.
- Nonsense mediated decay as well as disease mutations in RIα highlight the importance of this holoenzyme for regulating PKA signaling.
- Mapping these disease mutations reveals clustering at functional hot-spots that define either gain-of-function (CNC) or loss-of-function (ACRDYS) phenotypes.
- Crystal structure describes one of the dysfunctional ACRDYS mutants with a C-terminal deletion.

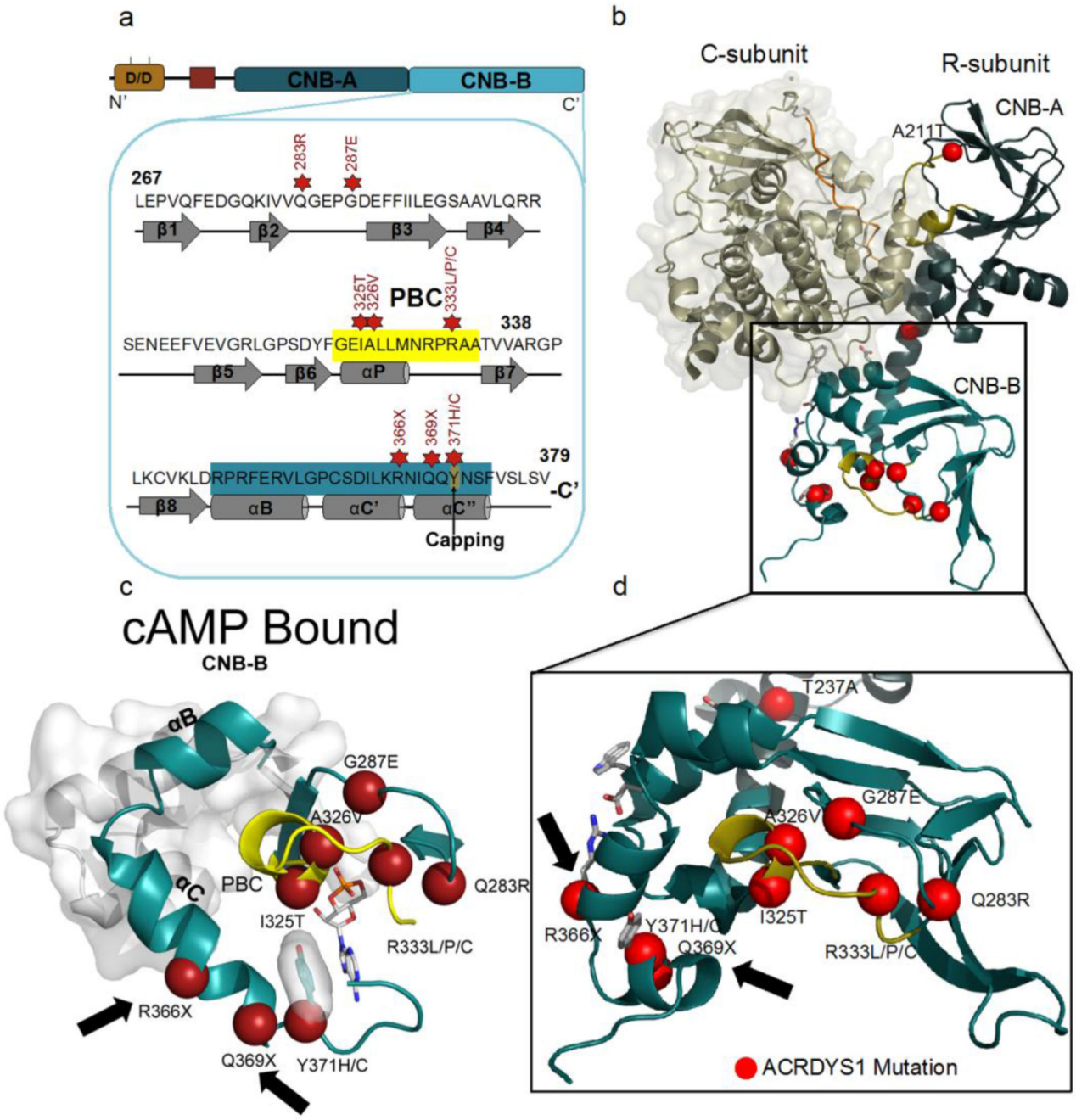

Figure 1. Structural map of RIα acrodysostosis-1 mutations

(**a**) Shows the domain organization of RIα with the CNB-B sequence and the locations of ACRDYS1 mutations (red stars). (**b**) The known ACRDYS1 mutations are mapped onto the RIα structure in the C-bound conformation (pdb 2qcs). Highlighting the CNB-B of RIα and the ACRDYS1 mutation locations in the cAMP-bound state (**c**) and C-bound conformation (**d**).

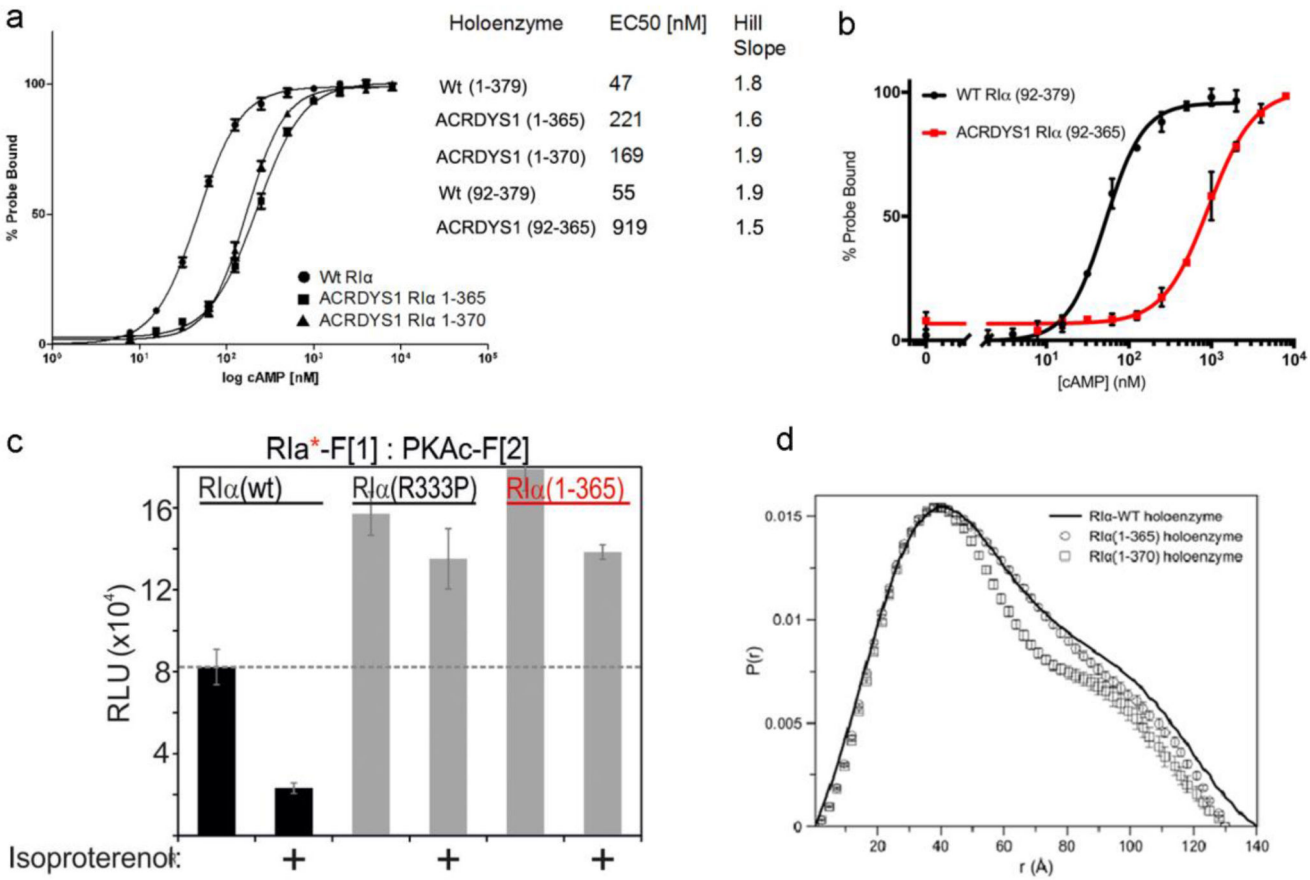

Figure 2. cAMP dependent activation of RIα ACRDYS1 complexes

(**a**) C-terminal deletion mutations of ACRDYS1 were analyzed with a fluorescent polarization assay to monitor changes in the ACRDYS1 mutant compared to wild-type holoenzymes ($RIα_2$:C_2). Activation profiles of holoenzyme formed with RIα wild type (circles), RIα 1-365 (squares) and RIα 1-370 (triangles) are shown. (**b**) Fluorescent polarization of the wild-type (black) and ACRDYS1 (red) heterodimers ($RIα_1$:C_1). GraphPad Prism was used to fit binding curves and the standard error of the mean is shown with error bars. (**c**) Combinations of wt and mutant *R*luc PCA tagged PKA subunits have been subjected to *R*luc PCA measurements. The effect of isoproterenol (1 μM; 15min) on complex formation of wild-type, ACRDYS1-mutant, and a control R333P PKA holoenzymes ($RIα_2$:C_2) has been determined using transiently transfected $β_2$AR-HEK293 cells (representative of at least n=3 independent experiments, ±SD from triplicates). (**d**) SAXS analysis of the ACRDYS1 $RIα_2$:C_2 complex. P(r) curves calculated from solution small-angle x-ray scattering data for RIα(1-365) mutant (circles) and RIα(1-370) mutant (squares). Wild-type P(r) curve is from Vigil et al. [43]. P(r) curves have been normalized to area under the curve.

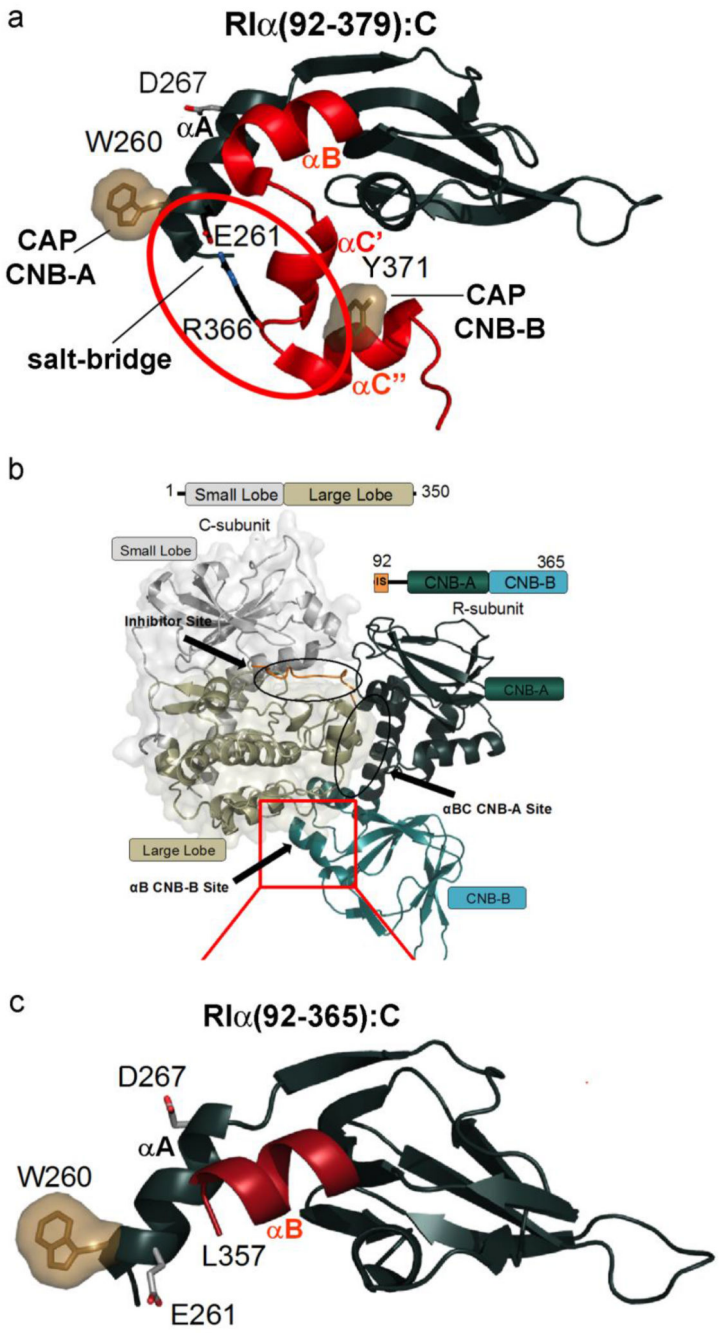

Figure 3. RIα ACRDYS1 heterodimer crystal structure

(**a**) The full-length RIα C-terminus in the R:C heterodimer conformation (pdb 2qcs) is shown and the red circle highlights several crucial residues including Arg366 and Tyr371. (**b**) Overall structure of the ACRDYS1 mutant RIα:C heterodimer. (**c**) In the ACRDYS1 Arg366stop mutant structure the residues beyond Leu357 are disordered.

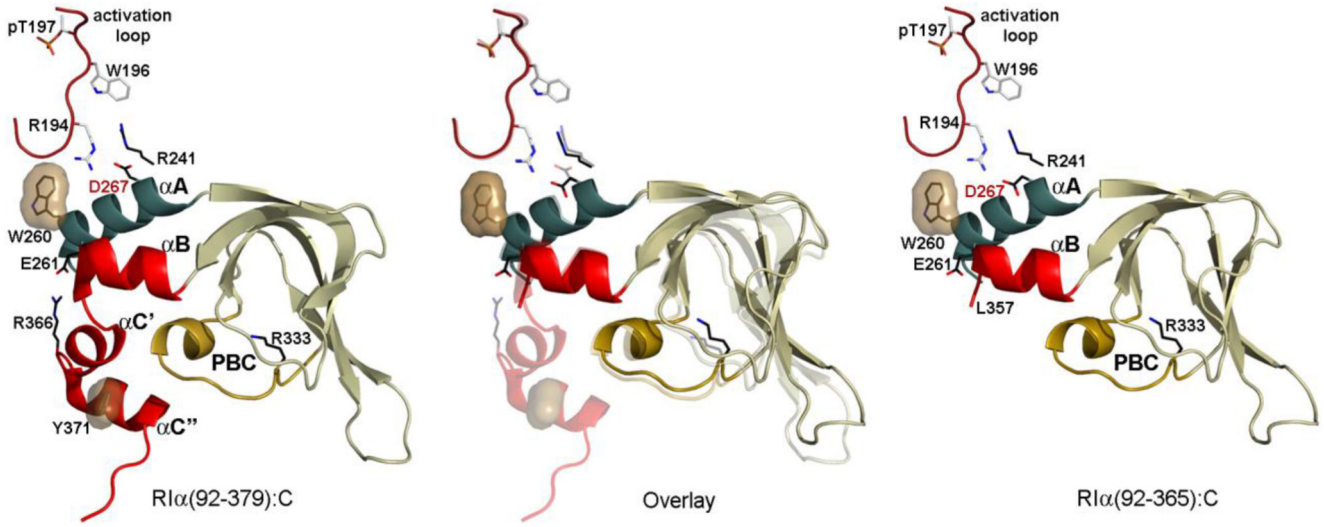

Figure 4. Comparison of the CNB-B capping motif

(left) In the holoenzyme conformation the kinked αC'/C"-helix contains the capping motif and includes Y371 and R366. **(middle)** The overlay of the full-length with the mutant structure highlights the missing regions as well as the lost connection to the activation loop. **(right)** This entire αC'/C"-helix, including Y371, is missing in the mutant as well as the holoenzyme specific R366 to E261 salt bridge. The interaction between R241 and D267 is also broken.

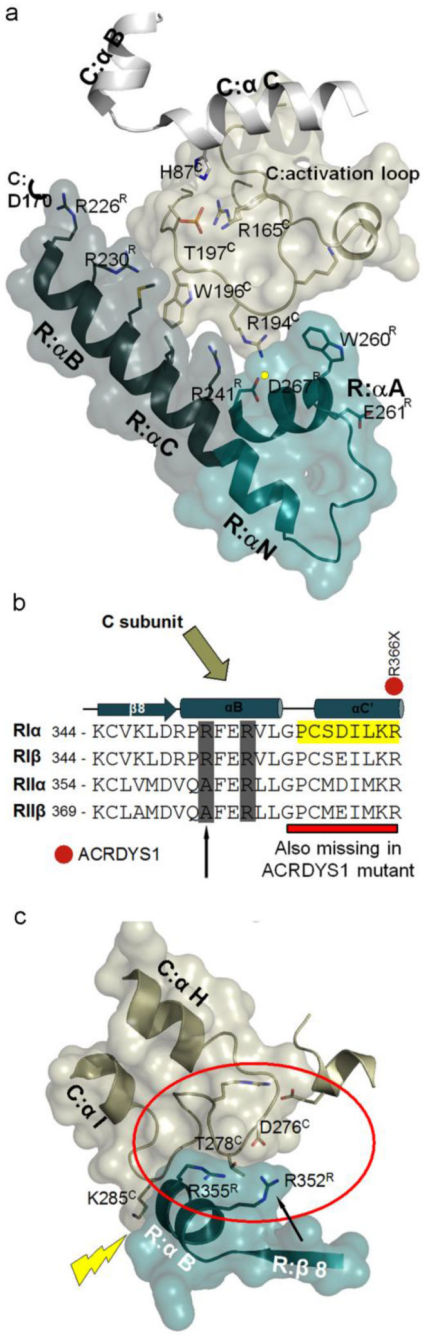

Figure 5. ACRDYS1 R:C-subunit interactions

(**a**) Zoom of the R:C interface between the CNB-A αBC-helix and the αA-helix of CNB-B. C-subunit residues are colored in olive and white. R-subunit residues are colored in dark and light green. (**b**) CNB-B αBC-helix sequence alignment of the R isoforms. Yellow highlights the ACRDYS1 residues disordered in this structure. (**c**) Zoom of the CNB-B αB-helix R:C interface with αH-αI loop of the C-subunit. Yellow arrow demonstrates initial point of PKA activation site.

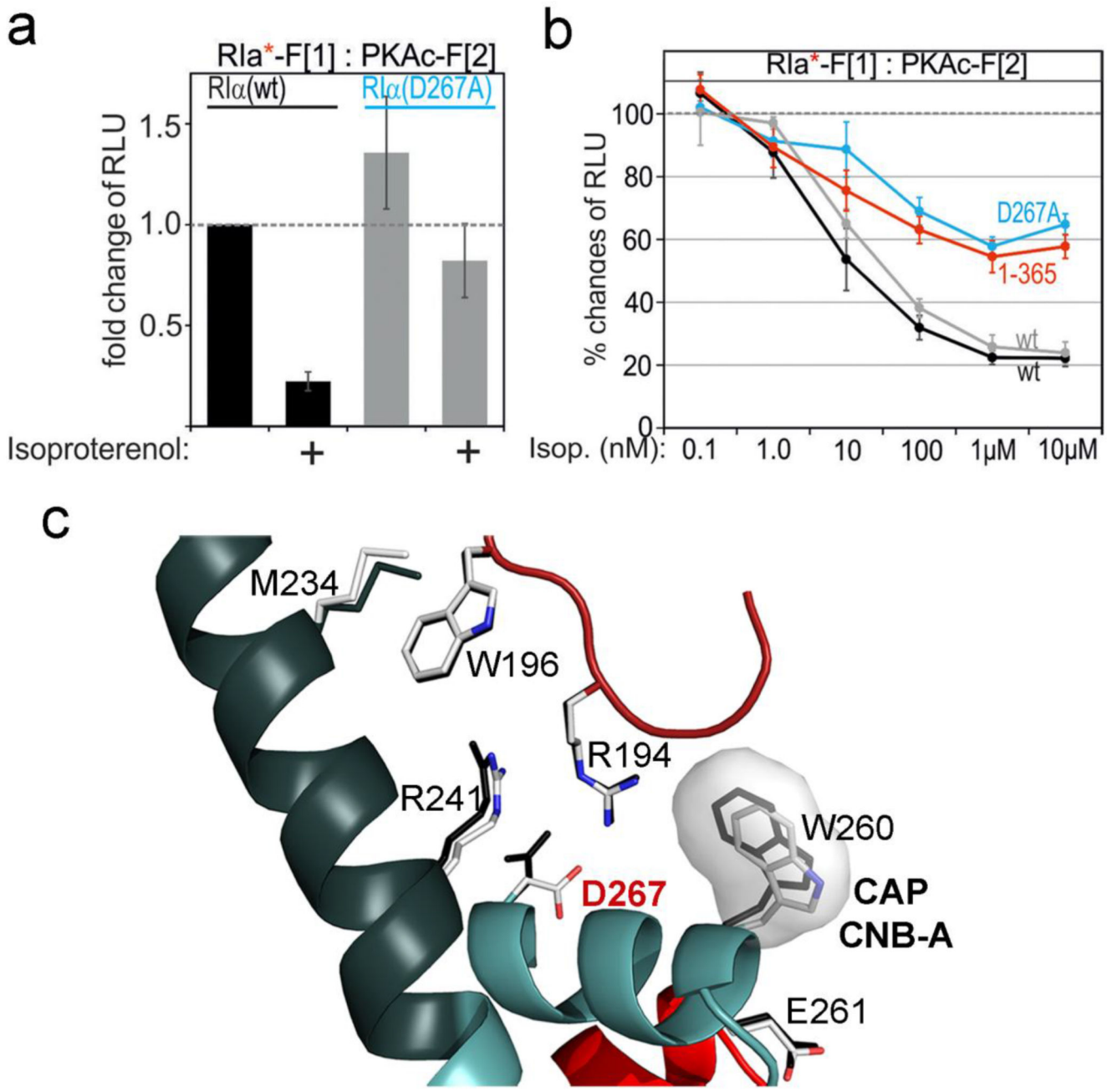

Figure 6. Importance of D267

(**a**) The effect of isoproterenol (1 μM; 15min) on complex formation of wt and D267A mutant PKA holoenzymes has been determined using transiently transfected β_2AR-HEK293 cells (representative of at least n=3 independent experiments, ±SD from triplicates). (**b**) The effect of isoproterenol (dose dependent; 15 min) on PKA complex formation of wt and ACRDYS1, and D267A RIα mutants has been determined using *R*luc PCA measurements (β_2AR-HEK293 cells; at least n=4 independent experiments, ±SEM).The PPI values have been normalized. Each if the control experiments (wt) has been performed in parallel to the mutant PKA holoenzyme PPI measurements. (**c**) Zoom of the D267/R241 pair which

nucleates the interaction to the activation loop of the C-subunit. The residues in 2qcs are shown in black.

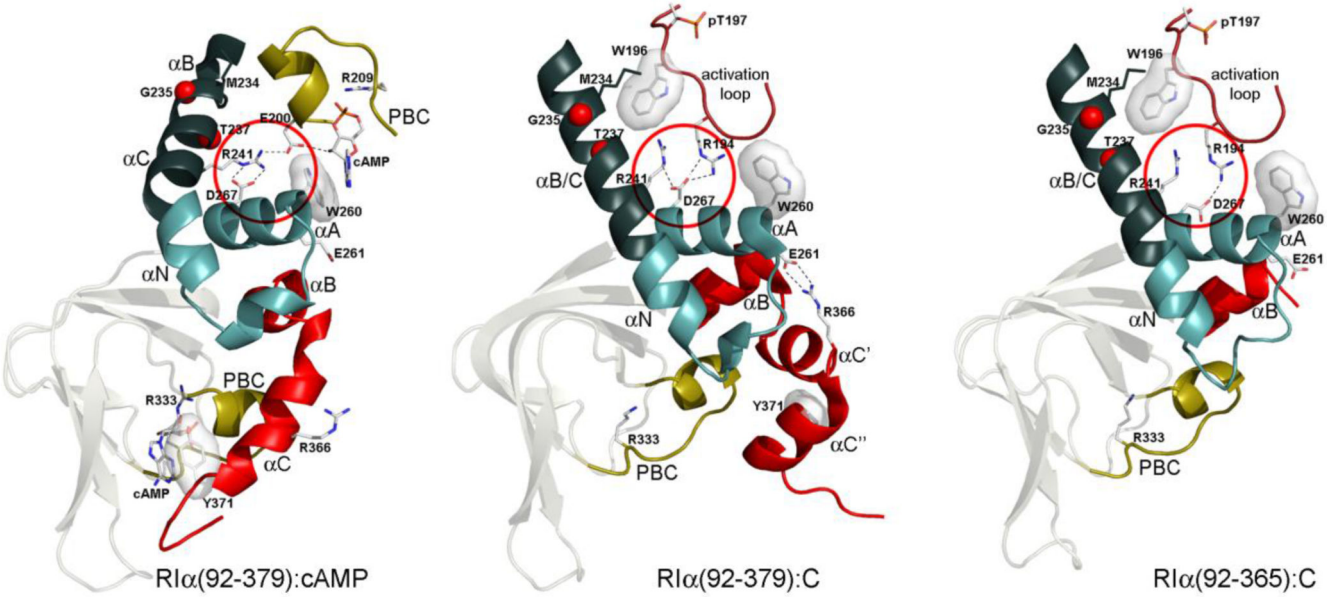

Figure 7. Allosteric network mediated by the αA-helix in CNB-B is disrupted in the ACRDYS1 mutant

(left) the cAMP-bound RIα shows R241 H-bonds to D267 as well as to cAMP via E200. However, E261 and R366 are both solvent-exposed. (middle) the C-bound full-length RIα shows the salt-bridge of E261-R366, while D267/R241 pair nucleate the interaction to Activation loop of C-subunit. (right) the C-bound ACRDYS1 mutant structure shows the loss of C-tail including R366 and changes in the interaction of D267/R241.

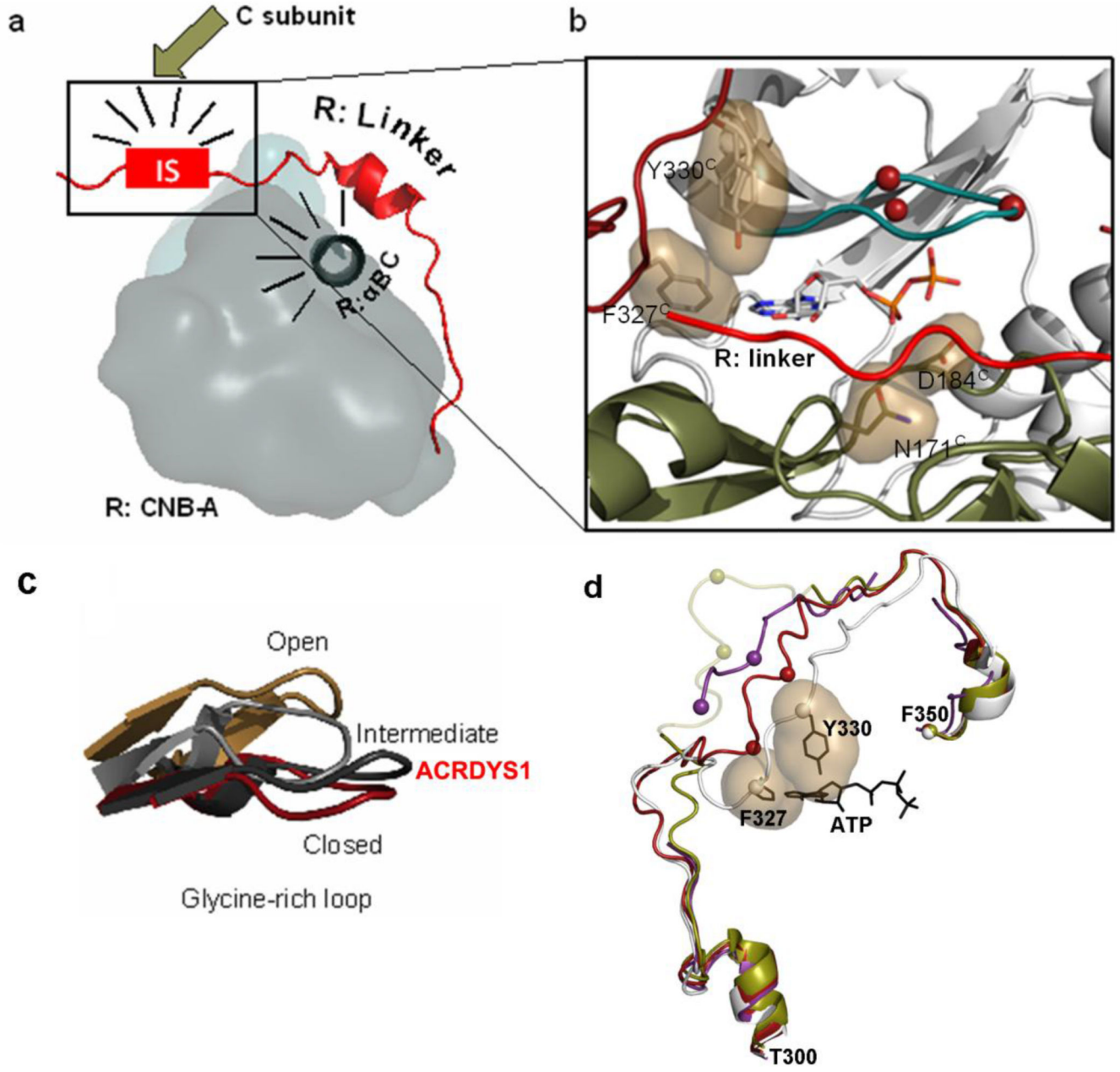

Figure 8. C-Subunit active-site comparison

(**a**) Cartoon of C-bound RIα highlighting the inhibitor site R:C interaction motif with arrow. (**b**) ACRDYS1 heterodimer structure is shown with a focus on the C-subunit active site. The C-lobe is colored in light olive and the N-lobe is colored in white. ADP is shown in stick representation and colored by element. The RIα linker is colored in red. (**c**) Glycine-rich loop comparison from alignment of the apo (brown, pdb 4NTS), intermediate ADP-bound (grey, pdb 4NTT), closed ATP-bound (red, pdb 1RDQ), and this ACRDYS1 (black) C-subunit structures. (**d**) C-tail comparison from alignment of the ACRDYS1 structure (purple) with the apo C subunit structure (tan, pdb 4NTS), the ADP:Mg bound C subunit structure (red, pdb 4NTT), and the ATP:Mg:PKI bound C subunit structure (grey, pdb 1ATP).

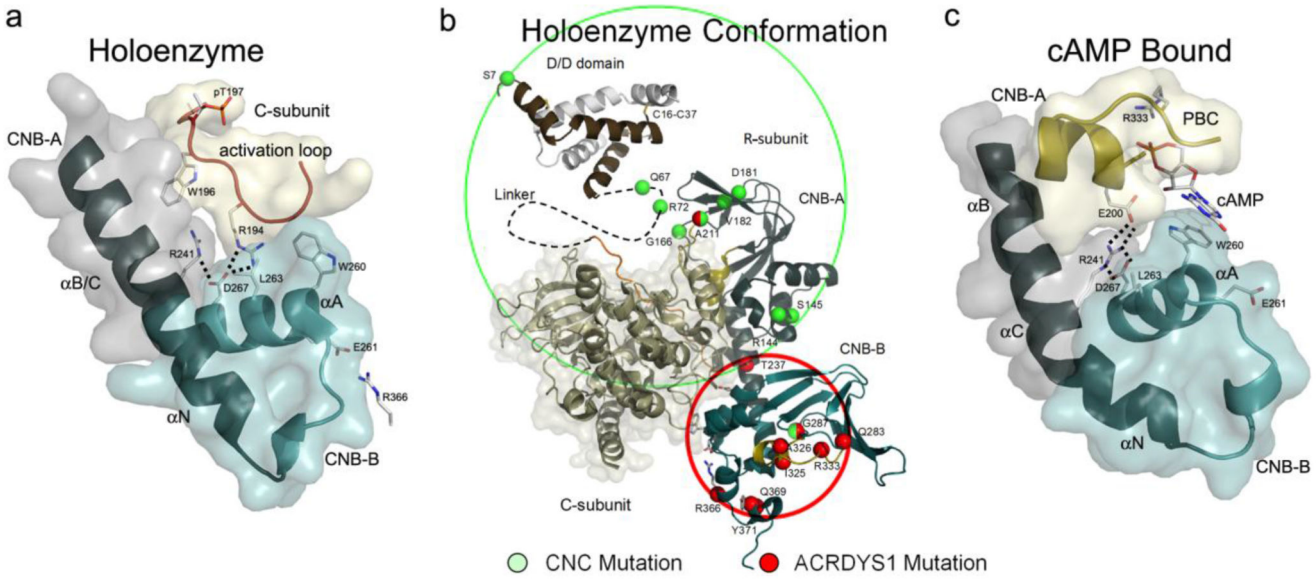

Figure 9. The helical rearrangements of the CNB-B and disease mutations of RIα

(a) The C-subunit bound state of RIα with a focus on the αA-helix interaction surface to the activation loop of the C-subunit. **(b)** Mapping of ACRDYS-1 mutations and CNC mutations on the RIα:C heterodimer structure shows they are structurally and functionally segregated to the CNB-B and CNB-A respectively. CNC mutations are shown with green spheres and acrodysostosis-1 mutations are shown as red spheres. Spheres that are half green/half red represent residues for which both an ACRDYS1 and a CNC mutation have been found. (**c**) The cAMP bound state of RIα with a focus on the αA-helix interaction surface to the cAMP in CNB-A. The images were made with pdb 2qcs and 1rgs with the CNB-A in dark teal, CNB-B in light teal, and the linker in orange. The C-subunit is shown in olive. The D/D domain in brown and white structure (pdb 3im3) relative position was modeled with the linker (dashed black line).